Reaction of OH with HO_2NO_2 (Peroxynitric Acid): Rate Coefficients between 218 and 335 K and Product Yields at 298 K

Elena Jiménez,[†,‡,§] Tomasz Gierczak,[†,‡,⊥] Harald Stark,[†,‡] James B. Burkholder,[†] and A. R. Ravishankara*[,†,#]

Aeronomy Laboratory, National Oceanic and Atmospheric Administration, 325 Broadway, Boulder, Colorado 80305-3328, and Cooperative Institute for Research in Environmental Sciences, University of Colorado, Boulder, Colorado 80309

Received: August 7, 2003; In Final Form: November 19, 2003

Rate coefficients ($k_3(T)$) for the reaction of OH with HO_2NO_2 (peroxynitric acid, PNA) in the gas phase were measured in the temperature range of 218−335 K by producing OH via pulsed laser photolysis and detecting it via laser-induced fluorescence. The PNA concentration was measured in situ by UV and IR absorption. The H_2O_2, HNO_3, and NO_2 impurities present in the PNA sample were quantified by mass spectrometry and/or UV/IR absorption. The measured value of k_3(298 K) is $(3.4 \pm 1.0) \times 10^{-12}$ cm^3 molecule^{-1} s^{-1}. The temperature dependence of k_3 is best described by the relation $k_3(T) = (8.8 \pm 2.6) \times 10^{-19} T^2 \exp[(1130 \pm 20)/T]$ cm^3 molecule^{-1} s^{-1}. The quoted errors for k_3 are at the 2σ level and include estimated systematic errors, which contribute the most to this uncertainty. The measured values of $k_3(T)$ were independent of pressure between 10 and 100 Torr of helium. The branching ratios of the reaction OH + HO_2NO_2 → products, for the production of HO_2 and HNO_3 and of NO_3 and H_2O_2, respectively, were determined to be <10% and <5%, respectively, at 298 K. Thus, it was deduced that the main pathway for reaction 3 produces H_2O, O_2, and NO_2 at 298 K. Our measurements reduce the uncertainties but do not significantly alter the currently calculated impacts of HO_2NO_2 in the upper troposphere and lower stratosphere. In the course of this study, the rate coefficient for the reaction of OH with H_2O_2 was measured to be $k_4(T) = (2.9 \pm 1.8) \times 10^{-12} \exp[-(110 \pm 150)/T]$ cm^3 molecule^{-1} s^{-1} in the temperature range of 273−356 K.

1. Introduction

Peroxynitric acid (HO_2NO_2, or PNA) has many roles in the Earth's upper troposphere and lower stratosphere (UTLS). First, it is a significant reservoir in the UTLS for both the HO_x (OH and HO_2) and NO_x (NO and NO_2) species.[1−3] Second, its formation couples the HO_x and NO_x families. Third, the reaction of OH with PNA is a significant sink for HO_x in the lower stratosphere (LS), unless HO_2 is a significant product of this reaction. For these reasons, HO_2NO_2 has an important role in determining the ozone abundance and its changes over time in the LS. Sequestering NO_x in HO_2NO_2 provides a mechanism for its redistribution in the upper troposphere (UT). Therefore, PNA also has a role in the formation of ozone in the UT.

Understanding the formation and loss processes of PNA under atmospheric conditions is critical in an evaluation of its role in ozone changes in the UTLS. PNA is formed in the atmosphere by the gas-phase association of HO_2 with NO_2:

$$HO_2 + NO_2 + M \leftrightarrow HO_2NO_2 + M \qquad (1,-1)$$

where M represents a third body. The formation reaction has been extensively studied over the past 20 years, and the rate coefficient for this reaction is reasonably well-established.[4] PNA is removed from the atmosphere by thermal decomposition, the reverse of reaction 1 (reaction (−1)),[5−7] photodissociation,[8−11] and its reaction with OH.[12−14]

$$HO_2NO_2 + h\nu \rightarrow \text{products} \qquad (2)$$

$$OH + HO_2NO_2 \rightarrow \text{products} \qquad (3)$$

Heterogeneous removal of PNA on or in atmospheric aerosols may also have a role. Each of these loss processes may contribute significantly to the atmospheric loss of PNA but may have differing impacts in the UTLS, in terms of the partitioning and removal of HO_x and NO_x. Thermal decomposition and near-infrared (NIR) photodissociation via overtone absorption[11] contribute to HO_x production at low light levels and will affect the partitioning of HO_x and NO_x. However, these processes do not remove OH, HO_x, and NO_x from the atmosphere. Reactive HO_x and NO_x species may be lost from the atmosphere via heterogeneous loss as well as via the reaction of OH with HO_2NO_2 and via UV photolysis, depending on the products of these two processes.

The rate coefficient for reaction 3 (k_3) has been previously measured in the laboratory by both relative[14,15] and absolute kinetic methods.[12,13] Fourier transform infrared (FTIR) spectroscopy,[12,15] FTIR and gas chromatography,[14] and modulated molecular beam mass spectrometry[13] were used in those experiments to measure the concentrations of PNA and the reactive impurities present in the PNA sample. The room-

* Author to whom correspondence should be addressed. E-mail: ravi@al.noaa.gov.
† National Oceanic and Atmospheric Administration.
‡ University of Colorado.
§ Current address: Departamento de Química Física. Facultad de Ciencias Químicas. Universidad de Castilla-La Mancha, Camilo José Cela, 10, 13071 Ciudad Real, Spain.
⊥ Permanent address: Department of Chemistry, Warsaw University, ul. Zwirki i Wigury 101, 02-089, Warsaw, Poland.
Also associated with the Department of Chemistry and Biochemistry, University of Colorado, Boulder, CO 80309.

10.1021/jp0363489 CCC: $27.50
Published on Web 01/24/2004

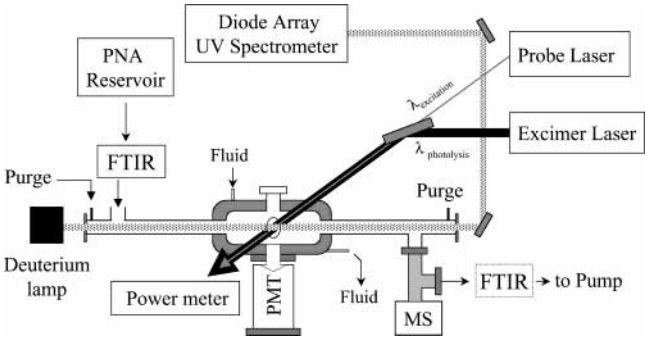

Figure 1. Schematic of the experimental apparatus used to measure rate coefficients for reaction 3. FTIR denotes the Fourier transform infrared spectrometer, MS represents the electron-impact ionization mass spectrometer, and PMT is the photomultiplier tube.

temperature values k_3 reported in these studies range from 4.0×10^{-12} cm^3 molecule^{-1} s^{-1} to 5.5×10^{-12} cm^3 molecule^{-1} s^{-1}. Such differences are not surprising, given the difficulties in determining the PNA concentration and accounting for the influence of reactive impurities. The temperature dependencies for k_3 reported by Barnes et al.,[14] Trevor et al.,[13] and Smith et al.[12] differ significantly. Barnes et al.[14] and Trevor et al.[13] reported k_3 to be essentially independent of temperature over the temperature ranges of 268−295 and 246−324 K, respectively. Smith et al.[12] reported a negative temperature dependence ($k_3(T) = 5.9 \times 10^{-13} \exp(650/T)$ cm^3 molecule^{-1} s^{-1}) over the temperature range of 240−330 K. Given the aforementioned discrepancies in the reported k_3 values, further kinetic studies under temperatures similar to those found in the UTLS are warranted.

In this work, absolute rate coefficients for the title reaction were measured at various temperatures by producing OH via pulsed laser photolysis (PLP) and detecting OH via laser-induced fluorescence (LIF). Emphasis was placed on quantifying the concentration of PNA and the impurities in PNA (H_2O_2, HNO_3, and NO_2) that react with OH. We also report the first laboratory determination of the product branching ratios for reaction 3:

$$OH + HO_2NO_2 \rightarrow H_2O + O_2 + NO_2 \quad (3a)$$

$$\rightarrow HO_2 + HONO_2 \quad (3b)$$

$$\rightarrow H_2O_2 + NO_3 \quad (3c)$$

2. Experimental Section

Measurements of the kinetics and products of reaction 3 involved recording OH temporal profiles using LIF, determining the concentrations of PNA (along with those of the reactive impurities HNO_3, H_2O_2, and NO_2), and monitoring the NO_3 concentration produced in reaction 3 via cavity ring down spectroscopy (CRDS). For ease of presentation, they are described separately in the three sections below.

2.1. Measurement of OH Temporal Profiles. Kinetics of OH removal was measured under pseudo-first-order conditions in the OH concentration between 218 and 335 K in 10−100 Torr of helium. The apparatus used for these measurements is shown schematically in Figure 1 and includes several modifications to that used recently in our laboratory.[16] The modifications enabled us to measure the concentration of the relatively unstable PNA in situ and quantify the concentrations of H_2O_2, HNO_3, and NO_2 that are unavoidably present in the PNA samples. These three molecules react with OH and, thus, contribute to the measured OH temporal profiles.

TABLE 1: Absorption Cross Sections and OH Quantum Yields[a]

λ (nm)	σ_λ (10^{-20} cm^2)	ϕ_{OH}
	HO_2NO_2	
193	900	0.26[b]
248	44	0.08[b]
	H_2O_2	
193	58.9	1.5
248	9	2
	HNO_3	
193	1160	0.33
248	2	1

[a] Values taken from Sander et al.[4] and references therein, unless noted otherwise. [b] Value taken from Jimenez et al.[31]

$$OH + H_2O_2 \rightarrow HO_2 + H_2O \quad (4)$$

$$OH + HNO_3 \rightarrow H_2O + NO_3 \quad (5)$$

$$OH + NO_2 + M \rightarrow HNO_3 + M \quad (6)$$

Whenever possible, multiple methods were used to determine the concentrations of PNA, H_2O_2, HNO_3, and NO_2 in the gas mixture. The PNA concentration was determined using two independent optical methods: (i) UV absorption using a diode array spectrometer and (ii) IR absorption using an FTIR spectrometer. H_2O_2, which is the reactive impurity in the PNA samples that contributed most to OH removal (other than PNA), was quantitatively measured using mass spectrometry (MS) and/or FTIR. HNO_3 was monitored via FTIR and by MS. NO_2 was monitored via UV absorption. Some details of the experimental hardware and methods are described below.

The reaction vessel has been described in detail previously.[16] It consisted of a 15-cm-long Pyrex jacketed cell with an internal volume of ~200 cm^3. The reactor was heated or cooled by circulating a fluid from a thermostated bath through its jacket. Orthogonal ports on the reactor were used to introduce the laser beams (collinear photolysis and probe beams), mount the photomultiplier detector, and allow sample gas flow through the reactor (see Figure 1).

Hydroxyl (OH) radicals were produced by excimer laser photolysis of a mixture of PNA and its impurities in the bath gas at 193 nm (ArF) or 248 nm (KrF). Photolysis of PNA, H_2O_2, and HNO_3 at these wavelengths produced OH. Therefore, the addition of an OH radical precursor was unnecessary. Table 1 summarizes the quantum yields for OH production in the photolysis of PNA, H_2O_2, and HNO_3 at 193 and 248 nm, as well as the cross sections of these molecules at these wavelengths. HNO_3 was the dominant OH radical precursor while using 193-nm photolysis. In the 248-nm photolysis experiments, the specific contributions of PNA, H_2O_2, and HNO_3 to the OH radical production were dependent on the PNA source and the experimental conditions. The photolysis laser fluence, which was measured with a power meter at the exit of the LIF cell, was varied between 0.08 and 2.5 mJ cm^{-2} pulse^{-1}. The initial concentration of OH radicals, $[OH]_0$, as estimated from the measured photolyte concentration, laser fluence, absorption cross sections, and the quantum yields, was kept below 5×10^{11} cm^{-3}, to minimize unwanted complications from secondary radical−radical reactions.

OH radicals were excited at ~282 nm ($A^2\Sigma^+, v' = 1 \leftarrow X^2\Pi, v'' = 0$) from the doubled output of a pulsed Nd:YAG-pumped dye-laser. The fluorescence signal was detected by a photomultiplier tube (PMT) oriented perpendicular to the

excitation beam. A band-pass filter (309-nm peak transmission; band pass of 20 nm fwhm (full width at half maximum)) mounted in front of the PMT was used to isolate the OH fluorescence from two transitions ($A^2\Sigma^+,\nu' = 1 \rightarrow X^2\Pi,\nu'' = 1$ and $A^2\Sigma^+,\nu' = 0 \rightarrow X^2\Pi,\nu'' = 0$). The OH temporal profiles were measured by varying the delay time between the photolysis and the probe laser pulses.

Rate coefficients for reaction 3 ($k_3(T)$) were measured under pseudo-first-order conditions in OH radical concentration ([reactant] > 1000 × $[OH]_0$). The OH temporal profile followed a simple exponential rate law:

$$[OH]_t = [OH]_0 \exp(-k't) \quad \text{(I)}$$

where $k' = k_3[PNA] + k_4[H_2O_2] + k_5[HNO_3] + k_6[NO_2] + k_7$ and k_7 is the first-order rate coefficient for the loss of OH in the absence of PNA, H_2O_2, HNO_3, and NO_2.

$$OH \rightarrow \text{loss} \quad (7)$$

The loss of OH in the absence of reactants is attributed to diffusion out of the detection zone and to reaction with impurities in the bath gas. The value of k' was measured at various concentrations of PNA at each temperature and pressure. Values of k_3 were obtained from the slopes of plots of $k' - (k_4[H_2O_2] + k_5[HNO_3] + k_6[NO_2] + k_7)$ vs [PNA]. Whenever possible, k_7 was derived by measuring the first-order rate coefficient for OH loss as a function of H_2O_2 under the same experimental conditions (temperature, pressure, and flow rates) just prior to the measurement of k_3; k_7 was the intercept in plots of the measured first-order rate coefficients for OH loss vs $[H_2O_2]$. Otherwise, $k' - (k_4[H_2O_2] + k_5[HNO_3] + k_6[NO_2])$ was plotted against [PNA] to obtain k_3 as the slope and k_7 as the intercept. The concentrations of PNA, H_2O_2, HNO_3, and NO_2 needed in the aforementioned analysis were measured using the methods described below, and the values of the k_5 and k_6 were taken from Brown et al.[17] and Wine et al.,[18] respectively. Because reaction 4 contributes the most to the measured value of k', k_4 was measured during the course of this study under the same conditions of pressure, temperature, and flow rate.

2.2. Measurement of PNA, HNO_3, H_2O_2, and NO_2 Concentrations. The concentration of PNA was measured via UV absorption using two 50-cm-long Pyrex cells coupled to two ends of the reaction cell, as shown in Figure 1. The windows on the Pyrex cells were flushed with a small amount of carrier gas, to limit contact with PNA, HNO_3, and H_2O_2. UV absorption was measured using a 30-W D_2 lamp light source and a 1024-element diode array detector.[19] The spectrograph was set to cover 200−450 nm, with a resolution of ~1.5 nm fwhm. The effective UV absorption path length under gas flow conditions of the kinetics studies was determined to be 114 ± 1 cm by flowing a known concentration of O_3 and measuring its absorption; this was essentially the same as the geometrical path length.

2.2.1. UV Absorption Measurements: The absorbance by a PNA sample at various wavelengths ($A_T(\lambda)$), as recorded by the diode array spectrometer, is the sum of the absorptions from PNA, H_2O_2, HNO_3, and NO_2:

$$A_T(\lambda) = A_{PNA}(\lambda) + A_{H_2O_2}(\lambda) + A_{HNO_3}(\lambda) + A_{NO_2}(\lambda) \quad \text{(II)}$$

The UV absorption spectra of PNA, H_2O_2, and HNO_3 are unstructured and overlap with each other. Therefore, the PNA concentration was not accurately determined from the UV absorption signal alone. Consequently, the concentrations of H_2O_2 and HNO_3 flowing through the cell were independently measured via MS and IR absorption measurements, as described below. The concentration of NO_2 was determined by the measured absorptions between 320 and 450 nm where PNA, HNO_3, and H_2O_2 do not absorb. The contributions of H_2O_2, HNO_3, and NO_2 to the measured UV absorption signal were subtracted to determine the UV absorption due to PNA. Absorption cross sections reported in the literature for PNA,[8] H_2O_2,[20] and HNO_3[21] were used in the spectral analysis. The reference spectrum for NO_2 in the UV region was recorded under the same experimental conditions (i.e., pressure and temperature) and approximately the same NO_2 concentrations observed in the PNA samples in the reactor. Under these conditions, there were no significant contributions to the measured absorption by N_2O_4. As shown in the Results and Discussion section, the typical contribution of H_2O_2 and HNO_3 to the total absorption signal at 250 nm was typically <10% and <4%, respectively. This value was 1%−50% for H_2O_2 and 1%−10% for HNO_3.

The UV absorption cross sections of PNA[8] and H_2O_2,[20] which are the two major contributors to the measured absorption, are relatively insensitive to temperature in the wavelength range of 240−300 nm. Therefore, the two 50-cm-long absorption cells attached to either end of the reactor were at room temperature while the temperature of the reactor was varied during the kinetic measurements. The differences in number density in the reactor and absorption cells due to differences in the temperature were taken into consideration in calculating concentrations of PNA and the other species.

The NO_2 concentration in the gas mixture flowing through the reactor was derived from the UV absorption measurements. The UV absorption cross sections of NO_2 are resolution dependent. Therefore, UV cross sections of NO_2 were measured under the conditions used for kinetic study by determining $[NO_2]$ via IR absorption measurements and recording the UV spectra. The obtained value of the absorption cross section at 414 nm was $(6.2 \pm 0.3) \times 10^{-19}$ cm^2 molecule^{-1}. Considering the differences in spectral resolution, it agrees with our previously measured value of 7.8×10^{-19} cm^2 molecule^{-1}.[22] The NO_2 concentration, as measured by UV or IR absorption in the reaction cell during the rate coefficient measurements, was in the range of 2×10^{13}−5×10^{14} molecules cm^{-3}. The NO_2 concentration was nominally ~5% of the PNA concentration.

2.2.2. Mass Spectrometric Measurements: A low-resolution mass spectrometer was used to monitor the H_2O_2 and HNO_3 concentrations at the output of the UV absorption cell; this instrument is described in our paper on UV absorption cross sections of PNA.[8] Parent ion signals were used to quantify the concentrations of both H_2O_2 ($m/z = 34$) and HNO_3 ($m/z = 63$). The mass spectrometer sampled the gas flow through a 40-μm pinhole (total reactor pressure of <20 Torr) or through a 15-μm pinhole (total reactor pressure of >20 Torr). Absolute calibrations of the MS signals for H_2O_2 and HNO_3 concentrations were made, relative to UV absorption measurements, just prior to the kinetic measurements. Calibrations were therefore performed under the identical flow and pressure conditions used in the kinetic measurements. The MS signals varied linearly with H_2O_2 and HNO_3 concentrations over the range observed in the kinetic measurements (8×10^{13}−1×10^{15} molecule cm^{-3} for H_2O_2 and 7×10^{13}−8×10^{14} molecule cm^{-3} for HNO_3; the HNO_3 concentrations were 5−10 times higher when PNA was generated using the H_2O_2/HNO_3 source).

2.2.3. Infrared Absorption Measurements: IR absorption spectra were recorded at room temperature using a Fourier

transform spectrometer between 500 and 4000 cm^{-1} at a spectral resolution of 1 cm^{-1} by co-adding 100 scans. A 15-cm-long, 1.5-cm-diameter, Pyrex absorption cell equipped with germanium windows was coupled to either the entrance or the exit of the UV absorption section (Figure 1). A capacitance manometer that was attached to a side port measured the pressure in the absorption cell. Reference IR spectra of H_2O_2, HNO_3, and NO_2 were measured in separate experiments. IR band intensities used to quantify the concentrations were taken from the HITRAN database.[23] The IR band intensities for PNA were taken from Smith and co-workers.[12,24] The PNA band intensities will be discussed further in the Results and Discussion section of this paper.

2.3. Measurement of NO_3 Product in Reaction 3 Using Cavity Ring Down Spectroscopy (CRDS). *2.3.1. Apparatus and Methodology.* The CRDS apparatus used for the NO_3 yield measurements is similar to one described previously.[25] A Nd:YAG laser pumped dye laser tuned to either 623 or 662 nm with a pulse duration of 6−8 ns was used to measure ring down signals. The intensity of light escaping from the rear mirror was collected by a PMT, digitized in an oscilloscope, and processed in a computer. The high-reflectivity mirrors used in this work resulted in empty cavity ring down time constants (τ_0) between 50 μs (at 623 nm) and 70 μs (at 662 nm). These τ_0 values correspond to mirror reflectivities of 99.994% and 99.996%, respectively.

The photolysis laser (KrF excimer laser, at 248 nm) beam was perpendicular to the ring down beam and illuminated 5 cm in the middle of the 100-cm-long cell. The ring down beam passed through the middle of this photolysis volume. The purge volumes efficiently suppressed contamination of the mirrors from exposure to corrosive gases such as PNA. The total pressure was varied between 25 and 40 Torr. An FTIR spectrometer was used to determine the concentrations of PNA, HNO_3, H_2O_2, and NO_2. The NO_3 radical was monitored at either 623 or 662 nm, where its absorption cross sections are 1.5×10^{-17} and 2.2×10^{-17} cm^2 $molecule^{-1}$,[26] respectively. All experiments were carried out at room temperature (296 ± 2 K). We calibrated the photon laser fluence in the reactor by detecting NO_3 that resulted from the photolysis of chlorine nitrate ($ClONO_2$) at 248 nm.

The technique of simultaneous kinetics and ring down (SKaR) was used in this study. In this technique, the ring down time of the optical cavity is comparable to the time constant for the reaction that changes the concentration of the monitored species. The ring down profiles in the absence and presence (with varying concentration of the absorber) are measured. The ratio of these two profiles contains the information on the time dependence of the absorber concentration. The analytical expression for the time dependence of the absorber concentration, together with the measured ratio of the profiles, is used to derive the rate coefficients and yields as described elsewhere.[25]

2.3.2. Materials. Helium (99.999%), N_2 (>99.99%), and NO_2BF_4 (> 95%) were used as supplied. Concentrated hydrogen peroxide (>95% H_2O_2, as determined by titration with a standard solution of $KMnO_4$) was prepared by bubbling N_2 through a H_2O_2 sample initially at a concentration of 60% for several days prior to use. Nitric acid (anhydrous) was synthesized under vacuum by slowly adding concentrated sulfuric acid to 40 g of solid $NaNO_3$ maintained at 330 K. HNO_3 vapor was collected in a glass bubbler immersed in a liquid N_2 cooled trap. $ClONO_2$ was prepared and used as described previously.[27]

Peroxynitric acid (PNA) was synthesized using two methods.[28] In the preferred method, PNA was prepared in solution by nitration of 8 cm^3 of concentrated H_2O_2 (>95%) at 273 K with 3 g of NO_2BF_4 in a glovebag purged with dry N_2. In the second method, PNA was prepared via a dropwise addition of 10 cm^3 of concentrated H_2O_2 to a stirred HNO_3 solution maintained at 0 °C. This second method had a tendency to leave behind large concentrations of H_2O_2 and HNO_3 and, therefore, was less suitable. PNA was introduced into the gas flow by passing a small flow of helium over the PNA solution while maintaining the reservoir at a temperature of 273 K. In the kinetic measurements, the sample gas flow was then passed through a cold trap immersed in a salt/ice bath to reduce the gas-phase H_2O_2 and HNO_3 concentrations.

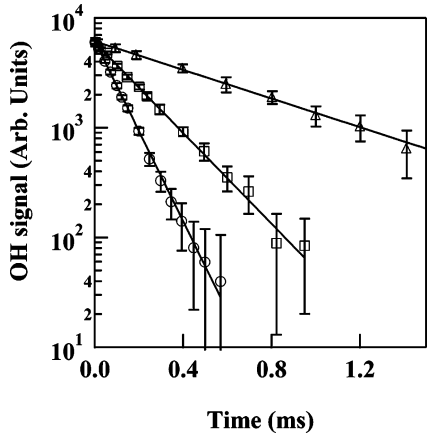

Figure 2. Typical OH temporal profiles recorded at 242 K in the presence of various concentrations of PNA: (○) 1.4×10^{15} molecule cm^{-3}, (□) 6.9×10^{14} molecule cm^{-3}, and (△) 2.1×10^{14} molecule cm^{-3}. Solid lines are weighted linear least-squares fits of the data to eq I.

Gas-flow rates were measured using calibrated mass flow transducers. The linear gas-flow velocity in the reaction cell used for OH kinetics was in the range of 10−76 cm s^{-1}; this flow rate was adequate to avoid an accumulation of photoproducts between photolysis laser pulses, which were 100 ms apart. Pressures were measured using 100 and 1000 Torr capacitance manometers. The temperature of the gas in the reaction zone was measured with a calibrated thermocouple inserted directly in the gas flow. The thermocouple was retracted during kinetic measurements. The flow rate of gases through the CRDS system was also sufficiently fast, so that the same gas mixture would not be exposed to more than one photolysis laser pulse; the pulse rate of the photolysis laser was 2−5 Hz.

3. Results and Discussion

Examples of OH temporal profiles measured in the rate coefficient studies of reaction 3 are shown in Figure 2. The OH loss followed first-order kinetics (i.e., obeyed eq I) over at least three of its lifetimes. Least-squares fits to the decay profiles yielded the k' values. PNA, H_2O_2, HNO_3, and NO_2 concentrations that corresponded to the measured k' value were determined from the ancillary measurements, as described in the Experimental Section. An example of the measured UV spectrum of the reaction mixture flowing through the reactor is shown in Figure 3. Based on the independently measured concentrations of the HNO_3 and H_2O_2 in this mixture and the reference spectra of these two species, their contribution to the measured spectrum are shown in Figure 3. As shown in this example, H_2O_2 and HNO_3 make relatively small (<10%) contributions to the UV absorption in the range of 240−290 nm. Thus, the PNA concentration is accurately determined in the UV absorption method. Therefore, even if the corrections

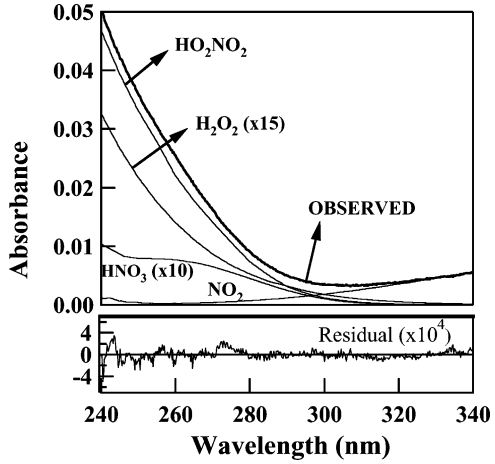

Figure 3. UV absorption spectrum of a gas-phase PNA sample flowing through the pulsed laser photolysis−laser-induced fluorescence (PLP−LIF) reactor. Spectrum was recorded using a diode array spectrometer with a path length of 114 cm. Also shown are the contributions of H_2O_2, HNO_3, and NO_2 to this absorption spectrum. The contributions due to H_2O_2 and HNO_3 were determined from auxiliary measurements of their concentrations via mass spectrometry and FTIR absorption. The NO_2 contribution was determined from its absorption at wavelengths longer than 340 nm and auxiliary FTIR measurements. In this example, the PNA, H_2O_2, HNO_3, and NO_2 concentrations are 1.2×10^{15}, 2.6×10^{14}, 6.1×10^{14}, and 2×10^{14} molecule cm^{-3}, respectively. The residual upon subtraction of all the contributions is shown at the bottom. Clearly, the residual is small (<1%) and shows no wavelength-dependent features.

due to H_2O_2 and HNO_3 are uncertain by 20%−30%, their contribution to the uncertainty in the PNA concentration is <5%.

Figure 4a shows examples of the measured first-order rate coefficient (k') vs [PNA] at 296 and 221 K. Figure 4b shows plots of $k' - (k_4[H_2O_2] + k_5[HNO_3] + k_6[NO_2] + k_7)$ values vs [PNA] at 298 K. The corrections applied to $k'(T)$, to account for the loss of OH due to reaction with H_2O_2, HNO_3, and NO_2, were typically 5%−25% of the measured value (see Figure 4a). The corrections for OH loss due to reaction with H_2O_2 and HNO_3 were smaller at lower temperatures. The major correction was due to reaction 4 (OH + H_2O_2) and ranged from 4% to ∼50%; the correction due to reactions 5 and 6 were typically <10% and 2%, respectively. Thus, the total correction was <25% and the uncertainty in the value of $k' - (k_4[H_2O_2] + k_5[HNO_3] + k_6[NO_2])$ due to the correction was <10%. Note that the derived value of k_3 was essentially independent of the magnitude of the correction for reactions 4−6, showing that the corrections were accurate.

The measured rate coefficient and conditions used in the OH experiments are summarized in Tables 2 and 3. A plot of k_3 (logarithmic scale) vs $1/T$ is shown in Figure 5. The rate coefficient data shows a slight detectable systematic deviation from Arrhenius behavior. However, note that the magnitude of the deviation lies within the absolute accuracy of the individual rate coefficient measurements. The kinetic data are well-reproduced over the entire temperature range using the rate coefficient expression

$$k_3(T) = AT^2 \exp\left(-\frac{E_a}{RT}\right) = (8.79 \pm 0.67) \times 10^{-19} T^2 \times \exp\left(\frac{1130 \pm 20}{T}\right) \text{cm}^3 \text{ molecule}^{-1} \text{ s}^{-1} \quad \text{(III)}$$

The quoted uncertainties are the 2σ values from the precision

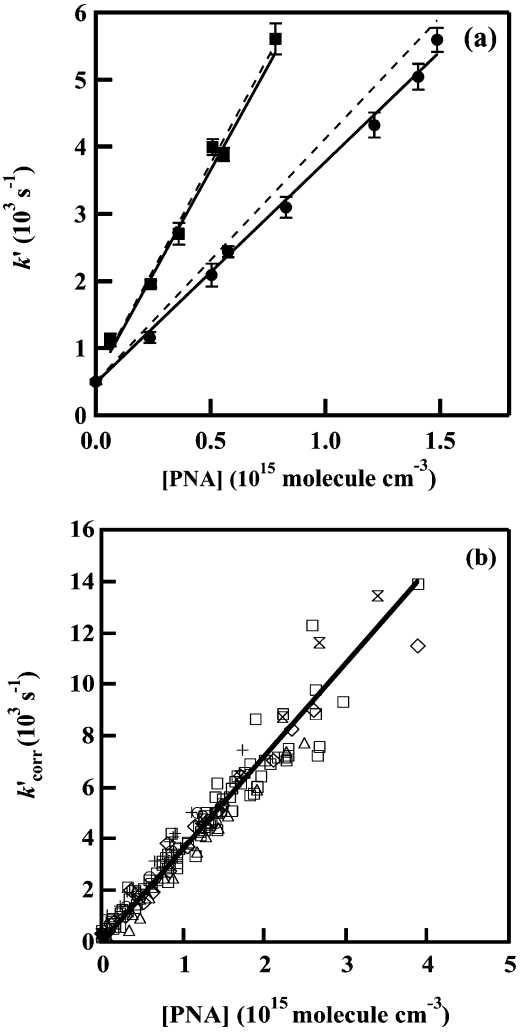

Figure 4. Plots of measured pseudo-first-order rate coefficients for the loss of OH in the presence of PNA (and its associated impurities), as a function of [PNA]. Panel a shows the data at 298 K (circles) and 221 K (squares). Solid lines are the weighted least-squares fits that take into consideration the contribution of the impurities, whereas the dashed lines represent the fits to the uncorrected data. Panel b shows a plot of the measured values of $k_{corr}' = [k' - (k_4[H_2O_2] + k_5[HNO_3] + k_6[NO_2] + k_7)]$ at 298 K (see Table 2), as a function of [PNA]. A weighted least-squares fit yields $k_3(298\text{ K}) = (3.44 \pm 0.12) \times 10^{-12}$ cm^3 molecule^{-1} s^{-1}.

of the nonlinear least-squares fit. Inclusion of the estimated systematic errors at the 2σ level in determining the concentration of PNA to the first term in the aforementioned expression will lead to $k_3(T) = (8.8 \pm 2.6) \times 10^{-19} T^2 \exp[(1130 \pm 20)/T]$ cm^3 molecule^{-1} s^{-1}. An Arrhenius fit, i.e., a fit of ln k_3 vs $1/T$ to a straight line using a linear least-squares analysis, to k_3 values measured at or below 298 K yields

$$k_3(T) = (3.18 \pm 0.30) \times 10^{-13} \times \exp\left(\frac{690 \pm 40}{T}\right) \text{cm}^3 \text{ molecule}^{-1} \text{ s}^{-1} \quad \text{(IV)}$$

where the quoted errors are 2σ and $\sigma_A = A\sigma_{\ln A}$. This expression reproduces the data well over this restricted temperature range (Figure 5). Again, inclusion of the estimated systematic errors at the 2σ level in determining the concentration of PNA into the first term in the aforementioned expression will lead to $k_3(T) = (3.2 \pm 1.0) \times 10^{-13} \exp[(690 \pm 40)/T]$ cm^3 molecule^{-1} s^{-1}.

TABLE 2: Summary of the Rate Coefficients for the OH + PNA Reaction at 298 K and Experimental Conditions Used To Measure Them

pressure (Torr)	gas flow velocity[a] (cm s^{-1})	photolysis laser fluence (mJ cm^{-2} pulse^{-1})	$[OH]_0$ (10^{11} molecule cm^{-3})	k_7 (s^{-1})	[PNA][b] (10^{15} molecule cm^{-3})	k' (s^{-1})	k_3(298 K)[c] (10^{-12} cm^3 molecule^{-1} s^{-1})
10	22	0.9−2.5	0.7−23.0		0.3−3.9 (8)	2200−14000	3.41 ± 0.68
14	29	0.4−0.7	0.4−1.8		0.2−1.8 (8)	600−5700	3.16 ± 0.24
14	30	0.6−2.1	0.1−1.1	470 ± 150	0.03−1.9 (11)	340−5600	3.19 ± 0.30
14	30	0.9	0.3−1.8	150 ± 25	0.2−2.6 (8)	1000−8800	3.59 ± 0.08
14	30	0.4−0.7	0.3−1.2	430 ± 55	0.1−3.2 (9)	500−9400	3.17 ± 0.10
14	30	0.4−1.0	0.5−1.8	680 ± 40	0.3−2.6 (9)	1700−7600	3.03 ± 0.08
14	30	0.4−1.0	0.6−2.0	630 ± 40	0.3−2.6 (9)	1700−7300	3.17 ± 0.08
14	30	0.1−0.3	0.05−1.0	690 ± 50	0.3−3.9 (9)	2000−11500	3.05 ± 0.12
14	72	0.1−0.2	0.03−0.2	400 ± 40	0.2−1.5 (7)	1200−5600	3.38 ± 0.12
14	26	0.1−0.2	0.05−0.5	280 ± 20	0.1−2.1 (7)	700−7000	3.37 ± 0.08
14	72	0.1−0.2	0.03−0.2	500 ± 20	0.2−1.5 (7)	1200−5600	3.29 ± 0.08
14	26	0.1−0.2	0.05−0.5	235 ± 30	0.1−2.1 (7)	700−7100	3.40 ± 0.06
15	50	2.7−3.1	0.3−5.4	200 ± 25	0.04−1.7 (10)	500−6500	3.77 ± 0.04
16	51	0.2−0.7	0.09−1.0	290 ± 20	0.1−1.4 (9)	700−5000	3.70 ± 0.08[d]
16	65	1.7−2.2	0.5−4.0	350 ± 30	0.06−1.7 (7)	1100−7400	3.82 ± 0.04 [e]
16	62	0.3	2.2−22	330 ± 20	0.2−1.5 (9)	1400−8000	3.27 ± 0.14[f]
17	53	0.7−1.4	0.4−3.6	290 ± 10	0.2−1.3 (5)	600−4600	3.18 ± 0.10
91	16	0.4−0.5	0.3−2.0	310 ± 10	0.1−3.4 (7)	200−13500	3.65 ± 0.04[d]
100	14	0.4−0.5	0.3−2.0	310 ± 10	0.4−2.5 (8)	1000−7700	3.24 ± 0.08
100	36	0.4−0.5	0.3−0.9	310 ± 10	0.3−1.6 (5)	500−5000	3.44 ± 0.16

[a] Gas flow velocity was calculated for the center of the reaction cell, where the OH temporal profiles were measured. [b] Number of PNA concentrations used in k_3 determination given in parentheses. [c] Uncertainties are the 2σ precision of the measurement values. [d] PNA source is HNO_3/H_2O_2 instead of NO_2BF_4/H_2O_2. [e] Photolysis wavelength, $\lambda = 193$ nm. [f] In the presence of 7×10^{15} molecules cm^{-3} of NO.

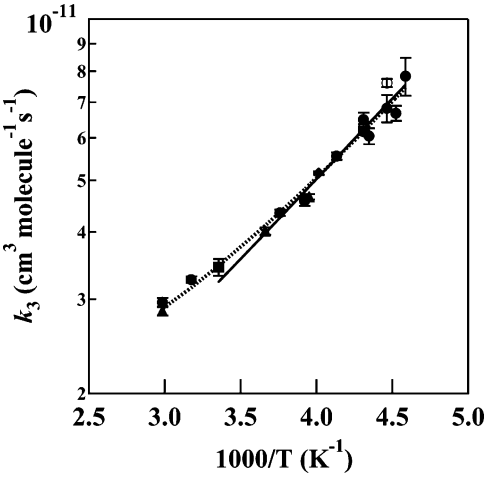

Figure 5. Plot of the k_3 value (on a logarithmic scale) from this work versus $1/T$. Dotted line is a weighted least-squares fit to the equation $k_3(T) = AT^2 \exp[-E_a/(RT)]$ and yields $k_3(T) = (8.79 \pm 0.67) \times 10^{-19} T^2 [\exp((1130 \pm 20)/T)]$ cm^3 molecule^{-1} s^{-1}. Solid line is a fit to the data at $T \leq 298$ K (shown in the figure over that range) to an Arrhenius expression, which yields $k_3(T) = (3.2 \pm 0.3) \times 10^{-13} \exp[(690 \pm 40)/T]$ cm^3 molecule^{-1} s^{-1}. All the quoted errors are 2σ precision obtained via least-squares analyses.

The experimental conditions were varied during the course of the kinetic experiments in an effort to identify potential systematic errors in the rate coefficient determinations. The majority of the experimental variations were performed at room temperature (see Table 2). The rate coefficient data was independent of the following: (i) the linear gas flow velocity ($v = 10-76$ cm s^{-1}) and the location of PNA addition to the apparatus; (ii) the PNA source, either $H_2O_2 + NO_2BF_4$ or $H_2O_2 + HNO_3$; (iii) the photolysis wavelength (193 or 248 nm); (iv) the initial OH radical concentration; and (v) total pressure (10−100 Torr of helium). This independence is demonstrated in the plot of all k' values measured at room temperature, as a function of [PNA] in Figure 4b. A linear least-squares fit of these data (a total of 168 first-order rate coefficients) yields $k_3(298\text{ K}) = (3.44 \pm 0.12) \times 10^{-12}$ cm^3 molecule^{-1} s^{-1}, where the quoted uncertainty is the 2σ precision of the slope of the k' vs [PNA] plot. If we include the estimated uncertainty at the 2σ level (see Section 3.1, "Error Analysis") in the determination of PNA concentration, we obtain $k_3(298\text{ K}) = (3.4 \pm 1.0) \times 10^{-12}$ cm^3 molecule^{-1} s^{-1}.

The range of temperatures over which we could accurately measure k_3 was limited at high temperature by the thermal decomposition of PNA (and the consequent uncertainties in the PNA concentration along the UV absorption cell) and at the low temperatures by condensation of PNA. We have established that our measured values of k_3 in the temperature range of 218−335 K were free of problems associated with uncertainties in PNA concentration and large contributions to the measured k_3 value by the presence of H_2O_2, HNO_3, and NO_2.

In a few experiments, under some specific conditions, the OH temporal profile was nonexponential and indicated a regeneration of OH at longer reaction times. Such OH regeneration was only observed when a freshly prepared PNA sample was first introduced into the reactor. We suspect that the regeneration was due to the presence of very small concentrations of NO that reacted with HO_2 radicals formed from PNA photolysis, reaction 4, or reaction 3b. An NO concentration of $\sim 1 \times 10^{13}$ molecule cm^{-3} is needed to explain the observed OH temporal profiles. Unfortunately, we were unable to detect such a small [NO] in our system. The addition of large concentrations of NO did make the OH temporal profiles exponential after 100 μs. Addition of very small amounts of NO made the profiles nonexponential. In any case, after flushing the bath gas through the PNA source for a few minutes, the OH regeneration was absent and all kinetic data were taken under such conditions.

3.1. Error Analysis. A major uncertainty in the determination of k_3 is associated with knowing the concentration of PNA in the reactor. We have used UV and IR absorption measurements to quantify the PNA concentration in our kinetic measurements. The UV measurements were performed within the reactor, whereas the IR measurements were external to the reactor. The UV and IR measurements yielded PNA concentrations that were within 10% of each other. Molina and Molina[10] and Singer et

TABLE 3: Summary of the Rate Coefficient for the OH + PNA Reaction, Obtained as a Function of Temperature (*T*)

T (K)	pressure (Torr)	gas-flow velocity[a] (cm s^{-1})	photolysis laser fluence (mJ cm^{-2} pulse^{-1})	$[OH]_0$ (10^{11} molecule cm^{-3})	k_7 (s^{-1})	[PNA][b] (10^{15} molecule cm^{-3})	k' (s^{-1})	k_3[c] (10^{-12} cm^3 molecule^{-1} s^{-1})
218	19	59	0.4−1.4	0.02−0.3		0.05−0.29 (5)	1300−3400	7.82 ± 0.64
221	20	60	0.9−0.9	0.05−0.5		0.06−0.62 (6)	1100−5600	6.67 ± 0.21
224	20	64	0.08−0.5	0.02−0.1		0.09−0.84 (6)	1000−4000	6.82 ± 0.40
224	95	10	0.3−0.3	0.1−0.3		0.06−0.80 (5)	1000−6000	7.59 ± 0.14
230	20	69	0.9−1.1	0.1−0.7		0.15−0.91 (5)	1200−5600	6.05 ± 0.21
232	19	55	0.2−0.3	0.05−0.4		0.09−1.10 (8)	700−6300	6.17 ± 0.10
232	20	67	0.5−0.7	0.05−0.6		0.07−0.91 (7)	1200−6100	6.49 ± 0.19
232	96	11	0.3−0.4	0.2−0.5		0.13−1.18 (8)	1400−8700	6.25 ± 0.11
242	15	38	0.1−0.2	0.02−0.4		0.07−1.70 (8)	800−9400	5.55 ± 0.09
249	16	48	1.3−1.8	0.8−2.5		0.50−1.73 (8)	2700−8600	5.16 ± 0.04[d]
253	15	47	1.7−1.8	0.3−1.5	320 ± 10	0.05−0.45 (8)	500−2400	4.66 ± 0.06[e]
255	14	27	0.4−0.4	0.04−0.8	440 ± 20	0.09−1.90 (11)	1000−8400	4.57 ± 0.10
266	15	33	0.4−0.4	0.04−0.8	420 ± 20	0.40−2.18 (8)	1600−9500	4.35 ± 0.06
273	17	48	0.5−0.5	0.1−1.0	390 ± 20	0.04−0.60 (8)	600−2700	4.02 ± 0.06[e]
298	10−100	14−72						3.44 ± 0.12[f]
315	13	33	0.5−0.5	0.06−0.4	140 ± 20	0.07−2.68 (8)	200−10000	3.26 ± 0.05
335	13	44	0.5−0.6	0.2−1.5	850 ± 25	0.23−2.56 (9)	1300−8500	2.96 ± 0.06
335	16	68	0.6−0.6	0.1−1.3	490 ± 30	0.31−0.85 (7)	1300−3000	2.85 ± 0.06[e]

[a] Gas-flow velocity was calculated for the center of the reaction cell, where the OH temporal profiles were measured. [b] Number of PNA concentrations used in k_3 determination given in parentheses. [c] Uncertainties are the 2σ precision of the measurement values. [d] In the presence of NO added. [e] PNA source is HNO_3/H_2O_2 instead of NO_2BF_4/H_2O_2. [f] Obtained from the slope of the plot of all k' values at 298 K versus [PNA] (see Figure 4b).

al.[9] estimated the uncertainty in the UV absorption cross section of PNA at 250 nm to be approximately ±10%. (Molina and Molina[10] quoted this to be at the 1σ level; we assume this to be at the 2σ level for the study by Singer et al.,[9] who did not specify their quoted uncertainty.) Uncertainties in the absorption path length, total pressure, temperature, and flows are all relatively small. The estimated uncertainty (approximately ±5%) in the UV spectral analysis, including uncertainties in the H_2O_2 and HNO_3 UV absorption cross sections, leads to an additional uncertainty in [PNA] of ∼10%. The calculated most-probable error in [PNA] that is due to uncertainty in the absorption cross sections, and accounting for contributions of H_2O_2 and HNO_3 to the measured absorbance, is estimated to be <20% at the 2σ level.

Several experiments were conducted to check the accuracy of the measured PNA concentration. In several experiments, the PNA concentration at the entrance and exit of the UV absorption cell were measured using IR absorption while measuring the concentration in the cell via UV absorption: they agreed to within ±10%, implying a lack of a gradient in the PNA concentration along the length of the UV absorption cell. Therefore, we conclude that the PNA concentration measured via UV absorption in the reactor is an accurate measure of the PNA concentration in the region where OH temporal profiles were measured. The PNA IR band intensities were determined, relative to the UV absorption measurements. The relative and absolute band intensities agreed well with those reported by Smith[24] and by Molina and Molina.[10] This agreement demonstrates a self-consistency between the UV and IR measurements made in these studies.

The PNA concentration was also indirectly measured by converting PNA to NO_2 in the presence of an excess of NO ($[NO] = (1.3-4.0) \times 10^{16}$ molecule cm^{-3}) at ∼532 K. A mixture of PNA, whose concentration was measured using UV absorption, and NO was passed through a heated (∼532 K) Pyrex tube. The PNA rapidly decomposed via reaction −1 to produce HO_2 and NO_2. The HO_2 radical formed in the PNA decomposition was converted to OH and NO_2:

$$HO_2 + NO \rightarrow OH + NO_2 \qquad (8)$$

TABLE 4: Reaction Mechanism Used in Simulations[a]

reaction	rate coefficient (cm^3 molecule^{-1} s^{-1}) k(298 K)[b]	k(532 K)[c]
Thermal Decomposition		
$HO_2NO_2 + M \rightarrow HO_2 + NO_2 + M$	0.013[d]	4498[d]
Hydroxyl Radical Reactions		
$OH \rightarrow$ loss	280[d,e,f]	
$OH + PNA \rightarrow H_2O + O_2 + NO_2$	3.6×10^{-12} [e]	2.1×10^{-12}[e]
$\rightarrow HO_2 + HNO_3$		
$\rightarrow H_2O_2 + NO_3$		
$OH + H_2O_2 \rightarrow HO_2 + H_2O$	2.0×10^{-12} [e]	2.15×10^{-12} [e]
$OH + NO_2 + M \rightarrow HNO_3 + M$	2.0×10^{-12}	4.9×10^{-14}
$OH + HNO_3 \rightarrow H_2O + NO_3$	1.3×10^{-13}	5.8×10^{-14}
$OH + NO + M \rightarrow HONO + M$	8.7×10^{-13} [e]	4.1×10^{-14}
$OH + HONO \rightarrow H_2O + NO_2$	4.5×10^{-12}	8.6×10^{-12}
HO_2 Radical Reactions		
$HO_2 + NO_2 + M \rightarrow HO_2NO_2 + M$	2.5×10^{-13}	7.5×10^{-15}
$HO_2 + NO \rightarrow OH + NO_2$	8.1×10^{-12}	5.6×10^{-12}
$HO_2 + HO_2 + M \rightarrow H_2O_2 + O_2 + M$	1.7×10^{-12}	7.1×10^{-13}
NO_3 Radical Reactions		
$NO_3 + NO \rightarrow 2\ NO_2$	2.6×10^{-11}	2.1×10^{-11}
$NO_3 + NO_2 + M \rightarrow N_2O_5 + M$	3.5×10^{-13}	3.8×10^{-14}
$NO_3 + HO_2 \rightarrow OH + NO_2 + O_2$	3.5×10^{-12}	3.5×10^{-12}

[a] Unless noted, the rate coefficients are taken from Sander et al.[4] [b] Pressure-dependent rate coefficients calculated for 45 Torr of helium. [c] Pressure-dependent rate coefficients calculated for 15 Torr of helium. [d] Units for this value are s^{-1}. [e] Measured in this study. [f] First-order loss rate coefficients measured in reaction cell via laser-induced fluorescence (LIF) detection of OH (see text).

which leads to the formation of another NO_2 molecule. The loss of OH via reaction 3a will produce yet another NO_2 molecule. Therefore, the loss of one PNA molecule leads to the formation of three NO_2 molecules. However, the efficiency of conversion of PNA to NO_2 will be slightly less than three, because of secondary chemistry of the OH radical (see the reaction mechanism listed in Table 4). The measured conversion efficiency of 2.5 is in good agreement with that expected from the reaction mechanism and the measured H_2O_2, HNO_3, PNA, NO, and NO_2 concentrations. This agreement adds to our confidence in the accuracy of the concentration of PNA measured via UV absorption.

TABLE 5: Summary of the Rate Coefficients for the OH + H_2O_2 Reaction[a]

temperature, T (K)	number of experiments	$[H_2O_2]$ (10^{14} molecule cm^{-3})	$[OH]_0$ (10^{11} molecule cm^{-3})	k_4' (s^{-1})	$k_4 \pm 2\sigma$ (10^{-12} cm^3 molecule^{-1} s^{-1})[b]
254	10	1.2−13.3	0.3−4.7	600−3200	2.16 ± 0.48
266	7	0.7−8.3	0.3−3.4	500−1825	1.86 ± 0.10
273	6	0.7−5.75	0.3−2.5	550−1550	1.99 ± 0.10
298	67[c,d]	0.8−16.5	0.1−25.0	600−3400	2.00 ± 0.08
315	6	2.4−13.3	1.3−6.5	680−3200	2.51 ± 0.10
335	11	0.9−25.4	1.5−9.3	550−5800	2.10 ± 0.26
356	20	0.5−22.2	0.1−2.2	635−4900	2.21 ± 0.38

[a] Pressure range was 13−16 Torr and H_2O_2 was photolyzed at 248 nm. [b] The quoted errors are 2σ precision of the linear least-squares fits of k_4' vs $[H_2O_2]$ data relative to the expression $k_4' = k_4[H_2O_2]$ + constant. [c] In 42 experiments, H_2O_2 was photolyzed at 193 nm. [d] One experiment was performed at 100 Torr.

TABLE 6: Comparison of OH + HO_2NO_2 Reaction Rate Coefficient Studies

temperature, T (K)	pressure (Torr)	k_3(298 K) (10^{-12} cm^3 molecule^{-1} s^{-1})[a]	A (10^{-12} cm^3 molecule^{-1} s^{-1})	E_a/R (K)	technique[b]	concentration measurement[c]	reference
218−335	10−100	3.4 ± 1.0	see text	see text	PLP/LIF	UV/MS/FTIR	this work
298	1	5.0[d]			relative rate	FTIR	Barnes et al.[15]
268−295	1−300	5.5 ± 1.4	independent of T		relative rate	FTIR/GC	Barnes et al.[14]
246−324	3−15	4.0 ± 1.6	8.05	(193 ± 194)	PLP/RF	MS	Trevor et al.[13]
240−330	760	5.2 ± 1.1	(0.59 ± 0.04)	−(650 ± 30)	PLP/RF	FTIR	Smith et al.[12]
		4.6	1.3	−380	evaluation		Sander et al.[4]

[a] Uncertainties reported by the authors. [b] PLP/LIF, pulsed laser photolysis/laser-induced fluorescence; PLP/RF, pulsed laser photolysis/resonance fluorescence. [c] UV, ultraviolet absorption spectroscopy; MS, mass spectrometry; FTIR, Fourier transform infrared spectroscopy; and GC, gas chromatography. [d] Revised in Barnes et al.[14] from the originally reported value of (4.1 ± 1.0) × 10^{-12} cm^3 molecule^{-1} s^{-1}, using (OH + propene) = 1.86 × 10^{-12} cm^3 molecule^{-1} s^{-1}.

A check of our methods was also accomplished through measurements of the rate coefficient for the reaction of OH with H_2O_2 (reaction 4). The summary of the measured rate coefficients for reaction 4 (k_4) and the conditions under which they were measured are given in Table 5. These rate coefficients were measured by monitoring the H_2O_2 concentration after the mass spectrometer was calibrated prior to most determinations of k_3. We obtained the value of k_4 in the temperature range of 254−356 K by fitting the ln k_4 vs $1/T$ data to a line using a weighted linear-least-squares methodology:

$$k_4(T) = (2.9 \pm 1.8) \times 10^{-12} \times \exp\left(-\frac{110 \pm 150}{T}\right) \text{cm}^3\,\text{molecule}^{-1}\,\text{s}^{-1} \quad \text{(V)}$$

Our data yields k_4(298 K) = (2.00 ± 0.15) × 10^{-12} cm^3 molecule^{-1} s^{-1}. The quoted errors in A and k_4(298 K) are at the 2σ level and include estimated systematic errors. These values of k_4 are in excellent agreement with the value reported by Vaghjiani et al.[29] These measurements were performed in the same system as that used for the determination of k_3 and using the same methods and the same conditions as those used to quantify the concentration of H_2O_2, i.e., MS determination. Therefore, this agreement further validates our determined concentrations of H_2O_2 and, more importantly, establishes the accuracy of the corrections made to k' for the contributions due to reaction 4, which was the largest contributor to the corrections.

As illustrated in Table 2, the precision of the individual k_3(298 K) determinations (approximately ±5%) is significantly better than the reproducibility of k_3 on different sets of determinations (±15%). This uncertainty, combined with our estimated uncertainty in [PNA] of ∼20%, leads us to estimate the overall maximum uncertainty in $k_3(T)$ to be ±30%. We believe that the precision of our measurements, to be conservative, is best-represented by the reproducibility of the measured values of k_3. Furthermore, this assignment of the precision accounts for the variations in the precisions of the corrections and the determinations of the PNA concentrations.

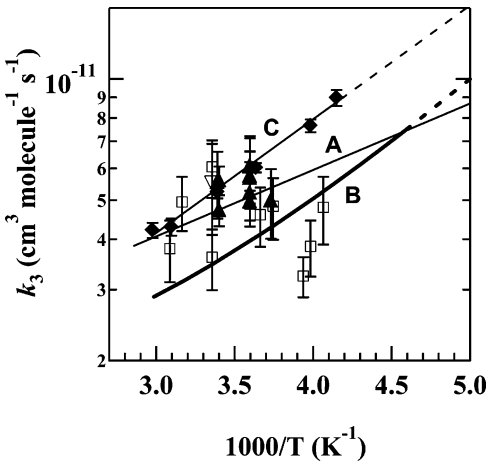

Figure 6. Comparison of the measured k_3 values with those from the previous work; this work (Line B), Barnes et al.[15] (open triangle), Barnes et al.[14] (solid triangles), Trevor et al.[13] (open squares), and Smith et al.[12] (solid diamonds). Line A represents the values recommended by Sander et al.[4] for atmospheric modeling. Line C represents the Smith et al. data. Dashed components represent extrapolation beyond the range of the measurements.

3.2. Comparison of $k_3(T)$ with Previous Studies. Graham et al.[6] published the first estimate of k_3(298 K), which was $< 3 \times 10^{-12}$ cm^3 molecule^{-1} s^{-1}; it was based on an indirect analysis of PNA thermal decomposition data. However, the more-recent "direct" measurements of k_3 (see Table 6 and Figure 6) have shown that the reported value of Graham et al.[6] is low. Our measured value of k_3(298 K) agrees with those determined using both relative rate[14,15] and absolute methods[12,13] within the quoted uncertainty limits. The independence of k_3(298 K) on pressure, in the pressure range of 10−100 Torr (helium), observed in this work also agrees with a similar lack of pressure dependence in the pressure ranges of 1−300 Torr (N_2) reported by Barnes et al.[14] and 3 and 15 Torr (helium) noted by Trevor et al.[13] Note that the scatter in the data of Barnes et al.[14] and Trevor et al.[13] is quite large and indicates the difficulty in measuring k_3. The precision of these measurements may not

reflect the real accuracy of their measurements. For example, the method used by Trevor et al.[13] to deduce their [PNA] value was rather indirect and would have led to significant variations from experiment to experiment. In the experiments where OH temporal profiles are measured, the largest contributors to the uncertainty in k_3 are the [PNA] and the contributions to OH loss by reaction with impurities. We have established our measured [PNA] value by multiple methods and have paid careful attention to the possible depletion of PNA along the length of the reactor. In contrast to the k_3 derived from OH temporal profile measurements, as in the case of Trevor et al.,[13] Smith et al.,[12] and us, the studies of Barnes et al.[14] do not suffer from the inaccuracies in [PNA] and impurity reactions, because they monitored the fractional depletion of PNA. Barnes et al.[14] had to account for secondary reactions and, thus, were not immune to other sources of error. Yet, the reasonable agreement between the reported values of Barnes et al.[14] and our study lends support to the quoted accuracy of k_3.

There are significant differences between the temperature dependence of k_3 reported by Barnes et al.,[14] Trevor et al.,[13] and Smith et al.[12] Barnes et al.[14] used an adaptation of the relative rate technique to determine $k_3(T)$ at 268, 278, and 295 K. They did not observe a statistically significant change in $k_3(T)$ over this narrow temperature range. Trevor et al.[13] used a laser photolysis resonance fluorescence technique to study reaction 3 at low pressure over the temperature range of 246−324 K. They observed a slightly negative temperature dependence on k_3. However, the overall low precision of their kinetic data limited them from defining the temperature dependence; they reported an E/R value of $-(193 \pm 194)$ K. The authors attributed the scatter in the data to possible wall reactions of OH and PNA in the flow tube. Uncertainties in the MS determination of [PNA] may also have contributed to the scatter. We expect the uncertainty in E/R to be less than that in A, because the largest sources of error in k_3 are the determination of [PNA] and corrections for impurities. This is to be expected because the thermal decomposition of PNA is not very rapid at and below 298 K and the rate coefficients for the other reactions that contribute to the measured OH loss (i.e., k_4, k_5, and k_6) are not very dependent on temperature over the range of temperatures studied.

Smith et al.[12] reported a systematic increase in k_3 with decreasing temperature in the temperature range of 240−330 K with a derived E/R value of −600 K, i.e., a negative temperature dependence. Our measured temperature dependence for k_3 is in good agreement with that reported by Smith et al.[12] However, the magnitude of the k_3 value reported by Smith et al. are systematically higher by ∼30% from our values. At present, we do not have an explanation for this discrepancy. One possible source of such a systematic difference is the corrections to the measured values of k', which is the first-order rate coefficient for a loss of OH, because of the presence of H_2O_2, HNO_3, and NO_2. Smith et al.[12] stated that their kinetic data corrections (in all cases) accounted for <30% of the measured k' values. This is not much different from the level of corrections to k' applied in our study. Smith et al.[12] used IR absorption to monitor the H_2O_2 and HNO_3 impurity concentrations, as was done in this work. They also used UV absorption to measure the PNA concentration, which is again similar to this work. The main correction to k_3 in our study is due to reaction 4, with minor contributions from reactions 5 and 6. In the study by Smith et al.,[12] the corrections due to reactions 5 and 6 were somewhat higher, because of the higher HNO_3 and NO_2 concentrations in their experiments. The k_6 values used by Smith et al.[12] to correct k' were measured in the same study in the temperature range of 240−370 K and the pressure range of 50−762 Torr of helium. The temperature and pressure dependence of the rate coefficient for reaction 6 has since been revised.[17] However, the revised values are not necessarily the best values to use for correction, because their measured values of k_4, k_5, and k_6 should be applicable to their system. The revised values would increase the magnitude of the corrections by ∼30%, i.e., increase the rate coefficient by ∼10%. Even such a correction, which may not be appropriate, probably will not be enough to completely account for the differences in the k_3 values. Note that even the uncorrected (raw) values of k' measured in this work would yield values of k_3 that are less than those reported by Smith et al.[12] Therefore, the discrepancies in our studies may not entirely be due to uncertainties in the corrections to k' or the quantification of [PNA].

The currently recommended value of $k_3(T)$ for stratospheric modeling is an average of the values reported by Barnes et al.,[14,15] Trevor et al.,[13] and Smith et al.[12] The recommended values are included in Figure 6 for comparison. The currently recommended[4] room-temperature value of k_3 is higher than our value. However, the values, when extrapolated to 200 K, only differ by ∼15% with our determination. This difference is well within the quoted, rather large, uncertainty. The implications of the results obtained in this work, which reduces the uncertainty in k_3 considerably, are discussed in Section 4, "Atmospheric Implications".

3.3. Product Measurements of the OH + HO_2NO_2 Reaction. The most likely reaction products, which are thermodynamically allowed, for the OH + PNA reaction are

$$\mathrm{OH} + \mathrm{HO_2NO_2} \rightarrow \mathrm{H_2O} + \mathrm{NO_2} + \mathrm{O_2} \quad (\Delta H^\circ_{298} = -45.8 \text{ kcal mol}^{-1}) \quad (3a)$$

$$\rightarrow \mathrm{HO_2} + \mathrm{HNO_3} \quad (\Delta H^\circ_{298} = -24.9 \text{ kcal mol}^{-1}) \quad (3b)$$

$$\rightarrow \mathrm{H_2O_2} + \mathrm{NO_3} \quad (\Delta H^\circ_{298} = -11.1 \text{ kcal mol}^{-1}) \quad (3c)$$

Currently, atmospheric models assume reaction 3a to be the only significant pathway. Reaction products of reaction 3a are difficult to detect in the laboratory, because of their high background concentrations in a PNA sample and the lack of a good way to measured H_2O and O_2 in a pulse photolysis system. In this work, we have measured the branching ratios for reactions 3b and 3c: reaction 3b through analysis of the OH temporal profile in the presence of NO and reaction 3c by direct measurement of the NO_3 radical. The branching ratio for reaction 3a is inferred from these values.

The branching ratio for reaction 3b ($\Phi_{3b} = k_{3b}/(k_{3a} + k_{3b} + k_{3c})$) was determined at $T = 298$ K by following the temporal profiles of OH in experiments that were identical to the kinetic measurements but with NO added to the sample. The addition of NO converts HO_2 radicals (produced either in the initial photolysis pulse or through subsequent reactions, e.g., reactions 3b and 4) to detectable OH radicals via reaction 8. Numerical simulations of the OH temporal profile using the chemical mechanism outlined in Table 4 and the measured experimental conditions were then used to estimate Φ_{3b}. An example of the measured OH temporal profiles in the presence of NO is shown in Figure 7. The increase in the OH signal at early times in the presence of NO results from the conversion of HO_2 produced in the photolysis of PNA at 248 nm.[30,31] The quantum yield for

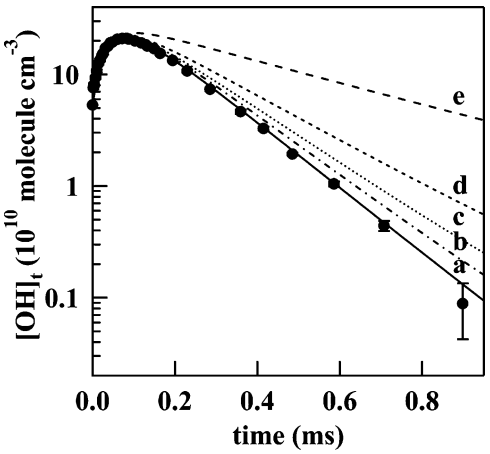

Figure 7. OH temporal profile observed following the pulsed photolysis of a sample that contained PNA (1.1×10^{15} molecule cm^{-3}), NO (2.3×10^{15} molecule cm^{-3}), and H_2O_2 (1.1×10^{14} molecule cm^{-3}). HNO_3 (2.1×10^{14} molecule cm^{-3}) and NO_2 (2.4×10^{14} molecule cm^{-3}) at 298 K. The lines represent simulations of the OH temporal profiles using the chemical mechanism given in Table 4 with the branching ratio for reaction 3b (Φ_{3b}) set equal to 0 (curve a), 0.1 (curve b), 0.2 (curve c), 0.4 (curve d), and 1.0 (curve e). This analysis clearly shows $\Phi_{3b} < 0.1$.

HO_2 in the 248-nm photolysis of PNA is reported to be >0.5. The rate of rise in the OH signal is determined by the NO concentration. The best fit to the OH temporal profile is obtained with $\Phi_{3b} = 0$. Simulations with several different Φ_{3b} are also shown in Figure 7 for comparison. We conclude from this analysis that Φ_{3b} is <0.10 and could be zero for the case shown in the figure. Such profiles at various concentrations of PNA and NO were measured and analyzed to derive an upper limit of $\Phi_{3b} < 0.1$.

The yield of NO_3 in reaction 3 (i.e., reaction 3c) was determined using the SKaR technique, as noted earlier. The measured CRDS profiles in the absence of OH production and upon OH production via 248-nm photolysis of a mixture of $PNA/HNO_3/H_2O_2$ are shown in Figure 8a. The concentrations of PNA, H_2O_2, HNO_3, and NO_2 were determined via IR absorptions. The reactions that occur in this system include the following:

$$HO_2NO_2 + h\nu\ (\lambda = 248\ \text{nm}) \rightarrow OH + NO_3 \quad (2a)$$

$$\rightarrow \text{other products} \quad (2b)$$

$$HNO_3 + h\nu\ (\lambda = 248\ \text{nm}) \rightarrow OH + NO_2 \quad (9)$$

$$H_2O_2 + h\nu\ (\lambda = 248\ \text{nm}) \rightarrow 2OH \quad (10)$$

and the reactions listed in Table 4. In this system, NO_3 radicals are produced via reaction 5 and also via reaction 3c. This mechanism can be further simplified to three processes of (i) the photolytic production of NO_3 that is coincident with the photolysis laser, (ii) the production of NO_3 as the reactions proceed, and (iii) the loss of NO_3 via reactions and physical removal:

$$HO_2NO_2 + h\nu\ (\lambda = 248\ \text{nm}) \rightarrow OH + NO_3 \quad (2a)$$

$$OH \rightarrow NO_3 \quad (11a)$$

$$\rightarrow \text{other losses} \quad (11b)$$

$$NO_3 \rightarrow \text{products} \quad (12)$$

Here, reaction 11 represents the loss of OH via its reactions with HO_2NO_2, HNO_3, NO_2, and H_2NO_2, whereas reaction 11a represents the loss of OH that leads to NO_3 formation via reactions with HO_2NO_2 and HNO_3. Reaction 12 represents the loss of NO_3 in this system. The pseudo-first-order rate coefficient for the production of NO_3 is equal to the pseudo-first-order OH loss rate coefficient and is given by

$$k_{11}' = k_3[HO_2NO_2] + k_4[H_2O_2] + k_5[HNO_3] + k_6[NO_2] + k_7 \quad \text{(VI)}$$

The rate coefficient for the loss of NO_3 was measured by monitoring the NO_3 concentrations at long times by varying the time delay between the photolysis and probe (CRDS) laser; k_{12}' was always <2000 s^{-1}. Because this loss is slower than the time scale of the ring down signal, we could not accurately quantify this rate coefficient in the SKaR profile. The overall pseudo-first-order rate coefficient for NO_3 production was on the order of 10 000 s^{-1} (i.e., the same time scale for the ring down signal); therefore, we use the SKaR method to measure the NO_3 production kinetics. This method has been described in detail in a previous publication from our laboratory.[25] Figure 8b shows the logarithm of the ratio of ring down signals with and without photolysis. The photolysis event is clearly identified at ~30 μs. Integration of the differential equation that represents reactions 2a, 11, and 12 yields the time dependence of the NO_3 concentration in this system, which is given by

$$[NO_3]_t = A \exp(-k_{11}'t) + B \exp(-k_{12}'t) \quad \text{(VII)}$$

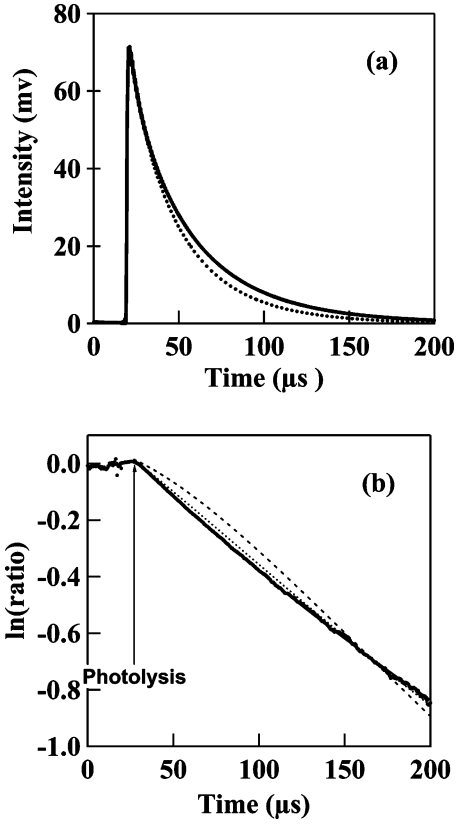

Figure 8. Cavity ring down spectroscopy (CRDS) profiles measured in the determination of the branching ratio for reaction 3c (Φ_{3c}). Panel a shows profiles measured in the absence of PNA (solid line) and in the presence of PNA (dotted line). Panel b shows the ratio of the two profiles shown in panel a (solid line); dashed lines are model simulations (see text for details) (with $\Phi_{3c} = 0\%$ (coincident with solid line), $\Phi_{3c} = 4\%$ (dotted line), and $\Phi_{3c} = 20\%$ (dashed line). The time of the photolysis is marked with an arrow.

Here, *A* and *B* are constants related to the initial concentrations of OH and NO_3. This temporal profile of NO_3 was included with the measured ratio profiles (such as that shown in Figure 8b) and the yield of NO_3 in PNA photolysis[31] to derive the yield of NO_3, as described elsewhere.[25] The calculated lines for various yields of NO_3 are also shown in Figure 8b. Several such experiments and analysis were performed to obtain an upper limit of <0.05 for the NO_3 yield in reaction 3.

We have measured upper limits for Φ_{3b} and Φ_{3c}. Assuming that there are no channels other than reactions 3a, 3b, and 3c for reaction 3, the lower limit for Φ_{3a} is quoted to be >0.85. Note that we really did not obtain a measurable value for reaction 3b or 3c, and, therefore, the branching ratio for reaction 3a to produce H_2O, O_2, and NO_2, could be 1.0.

4. Atmospheric Implications

The values of $k_3(T)$ at the temperatures of the upper troposphere and lower stratosphere (UTLS) are needed to evaluate the atmospheric lifetime of HO_2NO_2 and to elucidate the role of peroxynitric acid (HO_2NO_2, PNA) in affecting both the HO_x and NO_x budgets. Furthermore, because reaction 3 is a major sink for HO_x, its rate coefficient is needed to assess the HO_x loss rates and the stratospheric O_3 trends that are due to the anthropogenic emission of nitrogen oxides and halogen-containing molecules. The results from the present study significantly reduce the uncertainties in k_3. Our k_3 results are different from previously reported values; however, the differences from the values recommended for stratospheric modeling are not large. For instance, k_3(200 K) extrapolated using the results of this work is 1×10^{-11} cm^3 molecule^{-1} s^{-1}; this value is only ~15% lower than the current recommended value. Consequently, our results will lead to small changes in the calculated global lifetime of PNA in the UTLS and the impact on ozone trends. However, the uncertainty in these values that is due to uncertainties in the HO_2NO_2 chemistry is considerably reduced.

The product branching ratio measurements presented in this work are consistent with the current assumptions used in atmospheric model calculations. The main reaction channel leads to the formation of NO_2, O_2, and H_2O (reaction 3a). This reaction channel will lead to the net removal of HO_x in the UTLS:

$$HO_2 + NO_2 + M \rightarrow HO_2NO_2 + M \quad (1)$$

$$OH + HO_2NO_2 \rightarrow H_2O + NO_2 + O_2 \quad (3a)$$

$$\text{net reaction: } OH + HO_2 \rightarrow H_2O + O_2 \quad (13)$$

However, if reactions 3b and 3c were larger, reaction 3 would have been a smaller sink for HO_x in the lower stratosphere (LS). Recently, Salawitch et al.[32] suggested a few possible explanations for their inability to match the measured $[OH]/[HO_2]$ ratio in the LS with their model calculations. One possibility proposed was that k_3 was at the lower limit of the NASA/JPL recommendation[4] at the temperatures of the LS. Another possibility was that the branching ratio for reaction 3a was smaller than recommended. On the basis of our results, we excluded these two possibilities. Measurement of the product yields at temperatures that are characteristic of the LS would be beneficial.

Acknowledgment. This work was funded in part by NASA's Upper Atmospheric Research Program.

References and Notes

(1) Seinfeld, J. H.; Pandis, N. S. *Atmospheric Chemistry and Physics*; Wiley: New York, 1998.

(2) *WMO/UNEP Scientific Assessment of Ozone Depletion*: *1998* (Geneva, Switzerland); National Aeronautics and Space Administration: 1998.

(3) Finlayson-Pitts, B. J.; Pitts, J. N., Jr. *Atmospheric Chemistry*: *Fundamentals and Experimental Techniques*; Wiley: New York, 1986.

(4) Sander, S. P.; Finlayson-Pitts, B. J.; Friedl, R. R.; Golden, D. M.; Huie, R. E.; Kolb, C. E.; Kurylo, M. J.; Molina, M. J.; Moortgat, G. K.; Orkin, V. L.; Ravishankara, A. R. Chemical Kinetics and Photochemical Data for Use in Atmospheric Studies, Evaluation Number 14. *JPL Publ.* **2002**, *02*−*25*. (Available at the following URL: http://jpldataeval.jpl.nasa.gov.)

(5) Graham, R. A.; Winer, A. M.; Pitts, J. N., Jr. *Chem. Phys. Lett.* **1977**, *51*, 215.

(6) Graham, R. A.; Winer, A. M.; Pitts, J. N. *J. Phys. Chem.* **1978**, *68*, 4505.

(7) Zabel, F. *Z. Phys. Chem.* **1995**, *188*, 119.

(8) Knight, G.; Ravishankara, A. R.; Burkholder, J. B. *Phys. Chem. Chem. Phys.* **2002**, *4*, 1432.

(9) Singer, R. J.; Crowley, J. N.; Burrows, J. P.; Schneider, W.; Moortgat, G. K. *J. Photochem. Photobiol. A: Chem.* **1989**, *48*, 17.

(10) Molina, L. T.; Molina, M. J. *J. Photochem. Photobiol. A: Chem.* **1981**, *15*, 97.

(11) Roehl, C. M.; Nizkorodov, S. A.; Zhang, H.; Blake, G. A.; Wennberg, P. O. *J. Phys. Chem. A* **2002**, *106*, 3766.

(12) Smith, C. A.; Molina, L. T.; Lamb, J. J.; Molina, M. J. *Int. J. Chem. Kinet.* **1984**, *16*, 41.

(13) Trevor, P. L.; Black, G.; Barker, J. R. *J. Phys. Chem.* **1982**, *86*, 1661.

(14) Barnes, I.; Bastian, V.; Becker, K. H.; Fink, E. H.; Zabel, F. *Chem. Phys. Lett.* **1986**, *123*, 28.

(15) Barnes, I.; Bastian, V.; Becker, K. H.; Fink, E. H.; Zabel, F. *Chem. Phys. Lett.* **1981**, *83*, 459.

(16) Gierczak, T.; Gilles, M. K.; Bauerle, S.; Ravishankara, A. R. *J. Phys. Chem. A* **2003**, *107*, 5014.

(17) Brown, S. S.; Talukdar, R. K.; Ravishankara, A. R. *J. Phys. Chem. A* **1999**, *103*, 3031.

(18) Wine, P. H.; Kreutter, N. M.; Ravishankara, A. R. *J. Phys. Chem.* **1979**, *83*, 3191.

(19) Kegley-Owen, C. S.; Gilles, M. K.; Burkholder, K. B.; Ravishankara, A. R. *J. Phys. Chem. A* **1999**, *103*, 5040.

(20) Nicovich, J. M.; Wine, P. H. *J. Geophys. Res.* **1988**, *93*, 2417.

(21) Burkholder, J. B.; Talukdar, R. K.; Ravishankara, A. R.; Solomon, S. *J. Geophys. Res.* **1993**, *98*, 22937.

(22) Gierczak, T.; Burkholder, J. B.; Ravishankara, A. R. *J. Phys. Chem. A* **1999**, *102*, 877.

(23) Rothman, L. S.; Rinsland, C. P.; Goldman, A.; Massie, S. T.; Edwards, D. P.; Flaud, J.-M.; Perrin, A.; Camy-Peyret, C.; Dana, V.; Mandin, J.-Y.; Schroeder, J.; McCann, A.; Gamache, R. R.; Wattson, R. B.; Yoshino, K.; Chance, K. V.; Jucks, K. W.; Brown, L. R.; Nemtchinov, V.; Varanasi, P. *J. Quant. Spectrosc. Radiat. Transfer* **1998**, *60*, 665.

(24) Smith, C. A. The Atmospheric Reaction Kinetics of OH by Flash Photolysis−Resonance Fluorescence, Ph.D. Thesis, University of California, Irvine, CA, 1983.

(25) Brown, S. S.; Ravishankara, A. R.; Stark, H. *J. Phys. Chem. A* **2000**, *104*, 7044.

(26) Yokelson, R. J.; Burkholder, J. B.; Fox, R. W.; Talukdar, R. K.; Ravishankara, A. R. *J. Phys. Chem. A* **1994**, *98*, 13144.

(27) Yokelson, R. J.; Burkholder, J. B.; Fox, R. W.; Ravishankara, A. R. *J. Phys. Chem. A* **1997**, *101*, 6667.

(28) Kenley, R. A.; Trevor, P. L.; Lan, B. Y. *J. Am. Chem. Soc.* **1981**, *103*, 2203.

(29) Vaghjiani, G. L.; Ravishankara, A. R.; Cohen, N. *J. Phys. Chem.* **1989**, *93*, 7833.

(30) Roehl, C. M.; Mazely, T. L.; Friedl, R. R.; Li, Y.; Francisco, J. S.; Sander, S. P. *J. Phys. Chem. A* **2001**, *105*, 1592.

(31) Jiménez, E.; Gierczak, T.; Burkholder, J. B.; Stark, H.; Ravishankara, A. R. manuscript in preparation.

(32) Salawitch, R. J.; Wennberg, P. O.; Toon, G. C.; Sen, B.; Blavier, J. F. *Geophys. Res. Lett.* **2002**, *29*, 10.1029/2002GL015006.